

Astrometric detection of exoplanets

Fabo Feng^{a,b}

^aTsung-Dao Lee Institute, Shanghai Jiao Tong University, Shengrong Road 520, Shanghai, 201210, People's Republic Of China

^bSchool of Physics and Astronomy, Shanghai Jiao Tong University, 800 Dongchuan Road, Shanghai, 200240, People's Republic of China

© 2023 Elsevier Ltd. All rights reserved.

This is an update of F. Feng, Astrometric detection of exoplanets, Editor(s): Dimitri Veras, Snehil Sharma and Rajeswari R

1	Introduction	1
2	Types of astrometry	2
3	Detecting exoplanets with absolute astrometry	2
3.1	2D astrometry	2
3.2	1D astrometry	4
4	Detecting exoplanets with relative astrometry	5
4.1	Planet unresolved	5
4.2	Planet resolved	6
5	Sensitivity of astrometric exoplanet detection	6
6	Conclusions	7

Abstract

As the most ancient branch of astronomy, astrometry has been developed for thousands of years. However, it has only recently become possible to utilize astrometry for the detection of exoplanets. Gaia, an astrometric surveyor of 1 billion stars, is capable of measuring the position of stars with a precision as high as $20 \mu\text{as}$. Gaia is expected to discover more than 10,000 exoplanets by the end of its mission, surpassing the productivity of most exoplanet surveys.

In this chapter, I will introduce different techniques used to achieve high-precision astrometry. Subsequently, I will explore how both relative and absolute astrometry can be employed to detect exoplanets. Finally, I will present the detection limit of the Gaia astrometric survey.

Key points

- **Astrometry:** The precise measurement of stars' positions and their movements across the celestial sphere.
- **Exoplanet:** A planet orbiting a star other than the Sun.
- **Reflex motion:** The movement of a star around the center of mass of the entire system, comprising the star and its associated planets.
- **Parallax:** The apparent motion of a star caused by the observer's movement relative to the Sun.

1 Introduction

Astrometry is the specialized field of astronomy dedicated to the precise measurement of the positions and movements of celestial bodies. Millennia ago, ancient civilizations, including the Greeks, Babylonians, and Chinese, meticulously tracked the paths of planets and stars across the night sky. This practice resulted in the creation of early star maps, such as the catalog compiled by the Greek astronomer Hipparchus around 135 BC (Gysembergh et al., 2022) and the *Shi's Classic of Stars* (石氏星经) by Chinese astronomer Shi Shen (石申) in the 4th century BC (Ho, 2000).

In the late 16th century, Tycho Brahe conducted groundbreaking astrometric observations of approximately 1000 stars and planets. Johannes Kepler later compiled and published these observations in 1627 as the Rudolphine Tables. Kepler, utilizing these planetary astrometric data, went on to formulate the laws of planetary motion. In the 18th century, Sir William Herschel made significant contributions by discovering thousands of double stars, while Friedrich Bessel achieved a groundbreaking milestone by measuring the parallax of 61 Cygni with 9.6% precision. This marked

the first reliable measurement of the distance to a star beyond the solar system. The 19th-century introduction of photography revolutionized astrometry, as photographic plates enabled astronomers to capture and measure star positions with greater accuracy than traditional visual observations.

In 1989, the European Space Agency’s Hipparcos satellite was launched, conducting astrometric measurements for over a hundred thousand stars down to approximately 11th magnitude with unprecedented accuracy, reaching milli-arcsecond (mas) precision (Perryman et al., 1997). However, it was later surpassed by its successor, Gaia, which achieved even greater precision by measuring the positions of one billion stars with an accuracy as fine as 20 micro-arcsecond (μas ; Gaia Collaboration et al. 2016). Prior to Gaia, the detection and confirmation of exoplanets through astrometry were limited. An example is the determination of the mass of GJ 876 b, where astrometric data from the Hubble Space Telescope (HST) Fine Guidance Sensor (FGS) were analyzed (Benedict et al., 2002).

While the Gaia epoch data is currently pending release, researchers have already made significant strides in understanding exoplanets and substellar companions. Through the combined analysis of high-precision radial velocity data, along with astrometric data from Gaia and Hipparcos, the masses and orbital parameters of hundreds of exoplanets have been determined with remarkable precision (Snellen and Brown, 2018; Brandt et al., 2019; Kervella et al., 2019; Feng et al., 2022). Furthermore, Gaia Data Release 3 (DR3; Gaia Collaboration et al. 2023b) unveiled 64 new exoplanet candidates detected through astrometry (Gaia Collaboration et al., 2023a). In alignment with predictions by Perryman et al. (2014), Gaia is poised to revolutionize exoplanet discoveries, with expectations surpassing 10,000 newly detected exoplanets, heralding a new era in this field.

Gaia is primarily focused on sub-mas absolute astrometry, achieved through the observation of stars within a reference frame constructed by astrometric observations of compact extragalactic sources, such as more than one million quasars (Gaia Collaboration et al., 2022). Additionally, instruments like the optical interferometer FGS/HST and the infrared interferometer GRAVITY, integral to the Very Large Telescope Interferometer (VLTI), are capable of obtaining relative astrometry with a precision comparable to Gaia’s absolute astrometry. FGS/HST can measure positional changes between stars at a precision of about $200 \mu\text{as}$, while GRAVITY/VLTI excels in detecting finer changes, ranging from 10 to $100 \mu\text{as}$. Notably, GRAVITY achieved a remarkable $50 \mu\text{as}$ precision, determining the relative position of the renowned planet β Pic b and enabling accurate measurements of its mass and orbital parameters (GRAVITY Collaboration et al., 2020).

2 Types of astrometry

Astrometry involves the measurement of the position, motion, and parallax of celestial bodies. To quantify these parameters, a reference frame is established and realized through observations of distant objects, such as quasars. Surveys like Gaia and the Very-long-baseline interferometry (VLBI; e.g., Charlot et al. 2020) contribute to the establishment of absolute reference frames, enabling the determination of “absolute astrometry” (or global astrometry) for celestial bodies. In contrast, facilities like FGS/HST and GRAVITY/VLTI focus on measuring the relative motions between celestial bodies, known as “relative astrometry.” In relative astrometry, reference stars, usually distant stars, are chosen, and the target star’s motion is measured relative to them (e.g., Benedict et al. 2017).

Three primary astrometric techniques are imaging (e.g., HST Wide Field Camera), interferometry (e.g., GRAVITY/VLTI), and drift scan (e.g., Gaia). Imaging astrometry captures target images over multiple epochs, exemplified by the Cerro Tololo InterAmerican Observatory Parallax Investigation (CTIOPI; Jao et al. 2003), facilitating efficient astrometric determination. Interferometric astrometry utilizes interference patterns from telescopes or light paths, achieving higher angular resolution and detailed observation of fine celestial details. Unlike the other techniques, drift-scan astrometry does not track stars; instead, it allows stars to move across the detector over time, providing high precision astrometry directly linked to temporal information.

3 Detecting exoplanets with absolute astrometry

3.1 2D astrometry

For a planet with mass m_p orbiting a star with mass m_s , the reflex motion of the star relative to the mass center is given by:

$$\mathbf{r}_s(t) = \begin{bmatrix} x(t) \\ y(t) \\ z(t) \end{bmatrix} = \frac{m_p}{m_p + m_s} a \begin{bmatrix} \cos E(t) - e \\ \sqrt{1 - e^2} \sin E(t) \\ 0 \end{bmatrix}, \quad (1)$$

where a is the semi-major axis of the planet with respect to the star, $E(t)$ is the eccentricity anomaly, and e is the eccentricity. Here, m_p and m_s are respectively the mass of the planet and the host star, and m_s is typically determined through methods such as isochrone fitting or mass-luminosity relation. The semi-major axis for the reflex motion is

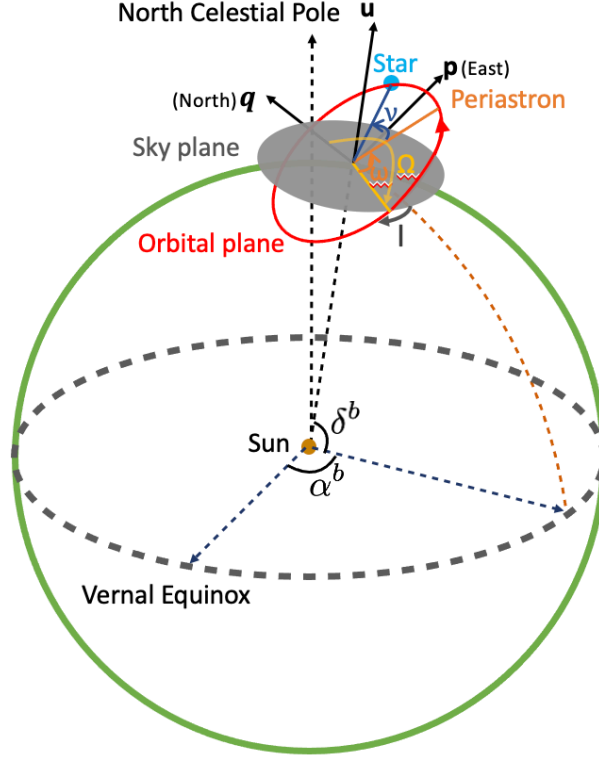


Fig. 1 Illustration of the coordinate system and orbital elements depicting stellar reflex motion (adapted from fig. 2 of Feng et al. 2019). The true anomaly ν represents the angle measured from the periastron to the star's position. The longitude of ascending node Ω is the angle measured from the North to the ascending node. The inclination I is the angle between the angular momentum of the orbital motion and $-\mathbf{u}$.

$$a_r = \frac{m_p}{m_p + m_s} a.$$

The stellar position $\mathbf{r}_s(t)$ is then converted to observer frame (sky plane) coordinates, $\mathbf{r}_s^{\text{obs}}(t)$, by applying Euler rotations using:

$$\mathbf{r}_s^{\text{obs}} = R_z(\Omega)R_x(-I)R_z(\omega)\mathbf{r}_s(t), \quad (2)$$

where Ω is the longitude of ascending node, ω is the argument of periastron, and I is the inclination of the stellar orbit with respect to the sky plane. It's important to note that the longitude of ascending node and the argument of periastron of the planetary (or secondary) motion should be $\Omega + \pi$ and $\omega + \pi$, respectively. In the observer's frame, the directions of the X axis (or \mathbf{q} , along North of the sky plane), Y axis (or \mathbf{p} , along East of the sky plane), and Z axis (or $-\mathbf{u}$, along the line of sight from the target to the observer) form a right-handed Cartesian coordinate system in the observer frame. This coordinate system corresponds to the first convention explained in the appendix of Feng et al. (2019). The orbital elements and coordinate systems are illustrated in Fig. 1.

The expansion of eq. 2 yields the observed location of the star in the XYZ coordinate system:

$$\begin{bmatrix} X(t) \\ Y(t) \\ Z(t) \end{bmatrix} = \begin{bmatrix} A' & F' & -\sin \Omega \sin I \\ B' & G' & \cos \Omega \sin I \\ -\sin \omega \sin I & -\cos \omega \sin I & \cos I \end{bmatrix} \begin{bmatrix} x(t) \\ y(t) \\ 0 \end{bmatrix}, \quad (3)$$

where

$$A' = \cos \Omega \cos \omega - \sin \Omega \sin \omega \cos I \quad (4)$$

$$B' = \sin \Omega \cos \omega + \cos \Omega \sin \omega \cos I \quad (5)$$

$$F' = -\cos \Omega \sin \omega - \sin \Omega \cos \omega \cos I \quad (6)$$

$$G' = -\sin \Omega \sin \omega + \cos \Omega \cos \omega \cos I \quad (7)$$

are the scaled Thiele-Innes constants (Thiele, 1883), functions of inclination I , argument of periastron of the target star ω , and longitude of ascending node Ω . Multiplying A' , B' , F' , G' by the semi-major axis of the reflex motion a_r defines

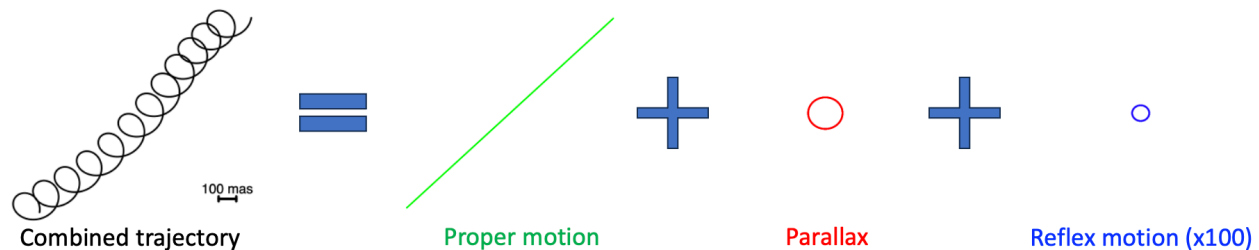


Fig. 2 Illustration showcasing different motions of a sun-like star when observed from a distance of 10 pc. The reflex motion induced by a Jupiter analog is enhanced by 100 times for optimal visualization. Proper motions in the R.A. and decl. directions are set at 100 mas.

the Thiele-Innes constants A, B, F, G . This assumes equivalence between the reflex motion and photocentric motion, as the planet’s contribution is negligible in moving the photocenter away from the host star. The decomposition of the stellar trajectory into proper motion, parallax, and reflex motion is illustrated in Fig. 2.

Hence, the reflex motion of the star in the directions of Right Ascension (R.A. or α) and Declination (decl. or δ) induced by a planet is given by:

$$\begin{aligned}\Delta\alpha_*^r(t) &= Y(t)/d = Bx(t) + Gy(t), \\ \Delta\delta^r(t) &= X(t)/d = Ax(t) + Fy(t),\end{aligned}\quad (8)$$

where $\Delta\alpha_* \equiv \Delta\alpha \cos \delta$ represents R.A. offset projected onto the sky plane, d is the heliocentric distance of the star. For multiple-planet systems, the total reflex motion is the sum of the reflex motion due to individual planets, assuming no N-body interaction between planets.

In addition to the reflex motion, the barycenter of the star-planet system is described by:

$$\begin{aligned}\alpha_*^b &= \alpha_{*\text{ref}}^b + \mu_\alpha^b(t - t_{\text{ref}}) + p_\alpha \varpi^b, \\ \delta^b &= \delta_{\text{ref}}^b + \mu_\delta^b(t - t_{\text{ref}}) + p_\delta \varpi^b,\end{aligned}\quad (9)$$

where $\kappa^b \equiv (\alpha_*^b, \delta^b, \varpi^b, \mu_\alpha^b, \mu_\delta^b)$ represents the 5-parameter barycentric astrometry at epoch t , and p_α and p_δ respectively represent the parallax factors in the R.A. and decl. directions. However, this model does not account for effects such as perspective acceleration and gravitational lensing (e.g., Klioner and Kopeikin 1992). As these effects are typically calculated a priori, they are subtracted from the raw data during a calibration procedure before conducting subsequent model fitting.

The complete astrometric model for a target is given by:

$$\begin{aligned}\hat{\alpha}_* &= \alpha_*^b + \Delta\alpha_*^r, \\ \hat{\delta} &= \delta^b + \Delta\delta^r.\end{aligned}\quad (10)$$

Typically, R.A. and decl. are measured relative to a reference position. Thus, the model and observation of the relative stellar position are represented as:

$$\begin{aligned}\hat{\zeta} &= (\Delta\hat{\alpha}_*, \Delta\hat{\delta})^T = (\hat{\alpha}_* - \alpha_{*\text{ref}}, \hat{\delta} - \delta_{\text{ref}})^T, \\ \zeta &= (\Delta\alpha_*, \Delta\delta)^T = (\alpha_* - \alpha_{*\text{ref}}, \delta - \delta_{\text{ref}})^T.\end{aligned}\quad (11)$$

When both R.A. and decl. of a star are measured, and the astrometric noise is Gaussian, the likelihood is defined as:

$$\mathcal{L}_{2D} = \prod_i^{N_{\text{epoch}}} [(2\pi)^2 |\Sigma_i|]^{-\frac{1}{2}} \exp \left\{ -\frac{1}{2} [\hat{\zeta}_i - \zeta_i]^T \Sigma_i^{-1} [\hat{\zeta}_i - \zeta_i] \right\}, \quad (12)$$

where N_{epoch} is the number of observation epochs, and Σ_i is the jitter-corrected covariance matrix of ζ_i . Specifically, $\Sigma_i \equiv \Sigma_{0i}(1 + J)$, where Σ_{0i} is the catalog covariance matrix for the i^{th} epoch, and J is referred to as “relative astrometry jitter.” This relative jitter accounts for unknown systematics in astrometric data.

3.2 1D astrometry

The drift-scan technique is commonly employed to enhance the efficiency of astrometric surveys, exemplified by the successful applications in the Hipparcos and Gaia missions. In this technique, the along-scan (AL) coordinate is approximately one order of magnitude more precise than the coordinate in the across-scan direction. The AL

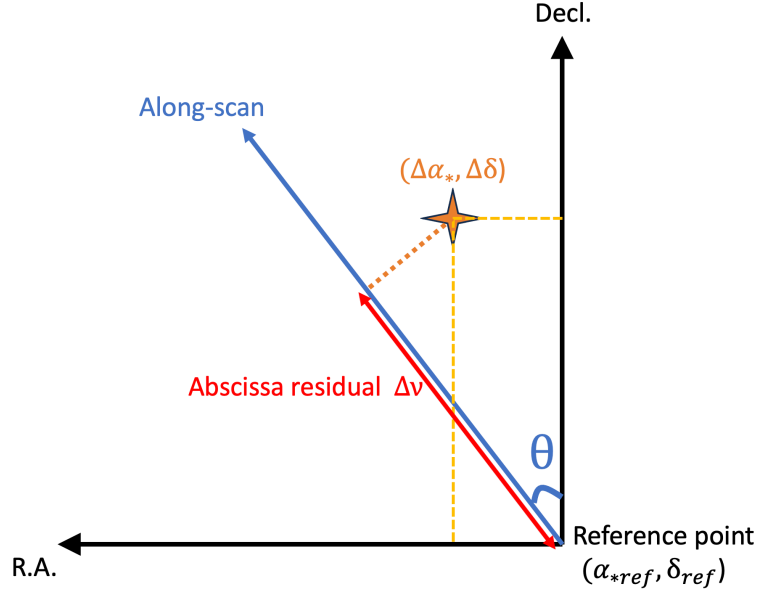


Fig. 3 Illustration of the conversion from R.A. and decl. to abscissa.

coordinate, referred to as the “abscissa,” is derived from the 2D model in eq. 10 by projecting the R.A. and decl. onto the AL direction (as depicted in Fig. 3):

$$\hat{\nu}_i = \hat{\alpha}_{*i} \sin \theta_i + \hat{\delta}_i \cos \theta_i, \quad (13)$$

where θ represents the scan angle¹.

Typically, the abscissae are defined as AL coordinates relative to the reference abscissa. Therefore, it is actually the abscissa residual. For a reference astrometry $\boldsymbol{\kappa}_{\text{ref}} = (\alpha_{*,\text{ref}}, \delta_{\text{ref}}, \varpi_{\text{ref}}, \mu_{\alpha,\text{ref}}, \mu_{\delta,\text{ref}})^T$ at the reference epoch t_{ref} , the abscissa residual is modeled as

$$\begin{aligned} \Delta \hat{\nu}_i = & [(\alpha_*^b + \Delta \alpha_{*i}^r - \alpha_{*,\text{ref}}) + (\mu_\alpha^b - \mu_{\alpha,\text{ref}})(t_i - t_{\text{ref}})] \sin \theta_i \\ & + [(\delta^b + \Delta \delta_i^r - \delta_{\text{ref}}) + (\mu_\delta^b - \mu_{\delta,\text{ref}})(t_i - t_{\text{ref}})] \cos \theta_i \\ & + (\varpi^b - \varpi_{\text{ref}}) p_i^{\text{AL}}, \end{aligned} \quad (14)$$

where $\boldsymbol{\kappa}^b = (\alpha_*^b, \delta^b, \varpi^b, \mu_\alpha^b, \mu_\delta^b)^T$ is the barycentric astrometry at the reference epoch, and p_i^{AL} is the AL parallax factor at epoch t_i . Defining Δt_i as $t_i - t_{\text{ref}}$ and the astrometric offsets $\Delta \boldsymbol{\kappa} \equiv (\Delta \alpha_*^b, \Delta \delta^b, \Delta \varpi^b, \Delta \mu_\alpha^b, \Delta \mu_\delta^b)$ as $\boldsymbol{\kappa}^b - \boldsymbol{\kappa}_{\text{ref}}$, the above equation becomes

$$\Delta \hat{\nu}_i = (\Delta \alpha_*^b + \Delta \alpha_{*i}^r + \Delta \mu_\alpha^b \Delta t_i) \sin \theta_i + (\Delta \delta^b + \Delta \delta_i^r + \Delta \mu_\delta^b \Delta t_i) \cos \theta_i + \Delta \varpi^b p_i^{\text{AL}}. \quad (15)$$

The corresponding likelihood for the above abscissa model is

$$\mathcal{L}_{\text{1D}} = \prod_i^{N_{\text{epoch}}} [2\pi(\sigma_i^2 + \sigma_j^2)]^{-\frac{1}{2}} \exp \left[-\frac{(\Delta \nu_i - \Delta \hat{\nu}_i)^2}{2(\sigma_i^2 + \sigma_j^2)} \right], \quad (16)$$

where σ_j is the jitter of abscissa, σ_i is the error of abscissa residual $\Delta \nu_i$.

4 Detecting exoplanets with relative astrometry

4.1 Planet unresolved

For a planet that is not resolved by imaging or interferometry, the reflex motion of its host star can be measured relative to distant reference stars in images taken at multiple epochs. All images (or plates) are adjusted to align

¹This definition of scan angle is consistent with Gaia, while $\psi = \pi/2 - \theta$ is the scan angle defined by Hipparcos.

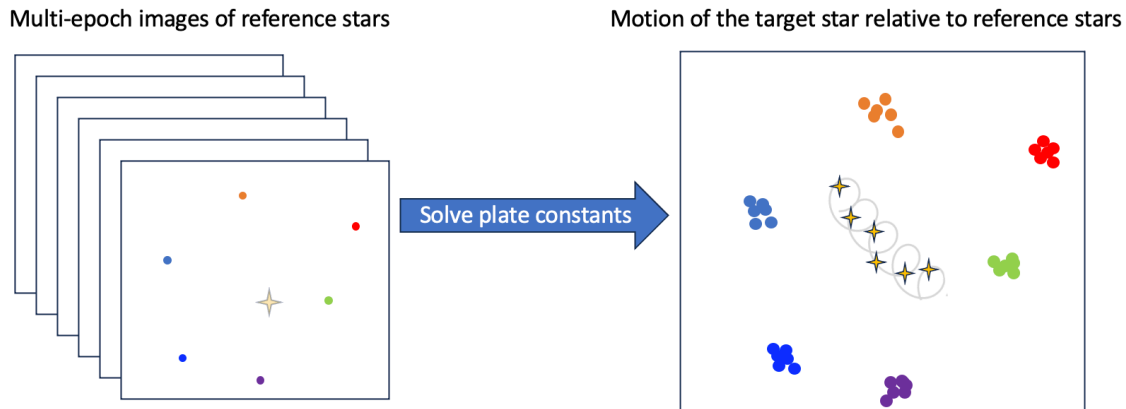


Fig. 4 Illustration of the relative astrometry for a star with an unresolved planet. The target star is not included in the process of plate solution.

with the R.A. and decl. directions using astrometric data from Gaia or Hipparcos². Additionally, the calibration for ground-based astrometry requires addressing the differential color refraction caused by atmospheric refraction (Jao et al., 2003). In FGS-like astrometry, the so-called “lateral color” resulting from the use of refractive optics is sometimes considered (Benedict et al., 1999). After calibration, the transformation of plates (or images) into a common frame, also known as a trail plate or constraint plate, is necessary.

For a reference star j in plate i with coordinates (x_{ij}, y_{ij}) , its coordinates in the constraint plate at epoch t_{ref} are given by:

$$\begin{aligned}\xi_{ij} &= a_i x_{ij} + b_i y_{ij} + c_i - \mu_{\alpha,j}(t_i - t_{\text{ref}}) - p_{\alpha,j} \varpi_j, \\ \eta_{ij} &= d_i x_{ij} + e_i y_{ij} + f_i - \mu_{\delta,j}(t_i - t_{\text{ref}}) - p_{\delta,j} \varpi_j,\end{aligned}\quad (17)$$

where $\beta^p = (a_i, b_i, c_i, d_i, e_i, f_i)^T$ are referred to as “plate constants,” t_i is the time when plate i is obtained. Assuming that the average relative parallax and proper motions are zero, the plate constants and astrometric parameters of reference stars are iteratively optimized, typically using the GaussFit algorithm developed by Jefferys et al. (1988). The principle of plate solution is illustrated in Fig. 4.

Once the plate parameters and astrometry of reference stars are solved, the parameters for the target star (represented by index 0) are determined by fixing these plate parameters at their optimal values. The coordinates of the target star in the constraint plate are

$$\begin{aligned}\xi_i &\equiv \xi_{i0} = a_i x_{i0} + b_i y_{i0} + c_i, \\ \eta_i &\equiv \eta_{i0} = d_i x_{i0} + e_i y_{i0} + f_i.\end{aligned}\quad (18)$$

The model for ξ_i and η_i is

$$\begin{aligned}\hat{\xi}_i &= \xi_0 + \mu_{\alpha,0}(t_i - t_{\text{ref}}) + p_{\alpha,0} \varpi_0 + \Delta\alpha_i^r, \\ \hat{\eta}_i &= \eta_0 + \mu_{\delta,0}(t_i - t_{\text{ref}}) + p_{\delta,0} \varpi_0 + \Delta\delta_i^r,\end{aligned}\quad (19)$$

where (ξ_0, η_0) is the reference coordinate of the target star in the constraint plate, $\Delta\alpha_i^r$ and $\Delta\delta_i^r$ are given in eq. 8. The corresponding likelihood is given by:

$$\mathcal{L}_{\text{unres}} = \prod_i^{N_{\text{epoch}}} [(2\pi)^2 |\Sigma_i|]^{-\frac{1}{2}} \exp \left\{ -\frac{1}{2} (\xi_i - \hat{\xi}_i, \eta_i - \hat{\eta}_i) \Sigma_i^{-1} (\xi_i - \hat{\xi}_i, \eta_i - \hat{\eta}_i)^T \right\}, \quad (20)$$

where Σ_i is the covariance of ξ_i and η_i . To model excess noise, the relative jitter J may be included to define the jitter-corrected covariance, $\Sigma_i \equiv \Sigma_{i0}(1 + J)$, where Σ_{i0} is the measured covariance.

4.2 Planet resolved

When a planet is resolved through direct imaging (e.g., Miles et al. 2023) or interferometric imaging (e.g., GRAVITY Collaboration et al. 2020), its host star serves as a reference star to derive the relative astrometry. The reflex motion

²In practice, the alignment has a small uncertainty. This uncertainty introduces second-order modeling uncertainty, which can be minimized through iterative optimization of plate constants and astrometric parameters of reference stars.

in eq. 8 is converted to the planetary motion using:

$$\begin{aligned}\Delta\hat{\alpha}_{*i}^p &= -\frac{m_s + m_p}{m_p}\Delta\alpha_i^r, \\ \Delta\hat{\delta}_i^p &= -\frac{m_s + m_p}{m_p}\Delta\delta_i^r.\end{aligned}\quad (21)$$

Defining $\zeta_i^p \equiv (\Delta\alpha_{*i}^p, \Delta\delta_i^p)^T$, and $\hat{\zeta}_i^p \equiv (\Delta\hat{\alpha}_{*i}^p, \Delta\hat{\delta}_i^p)^T$, the corresponding likelihood is

$$\mathcal{L}_{\text{res}} = \prod_i^{N_{\text{epoch}}} [(2\pi)^2 |\Sigma_i|]^{-\frac{1}{2}} \exp \left\{ -\frac{1}{2} (\zeta_i^p - \hat{\zeta}_i^p)^T \Sigma_i^{-1} (\zeta_i^p - \hat{\zeta}_i^p) \right\}, \quad (22)$$

where Σ_i is the covariance of ζ_i^p . If the separation ρ_i and position angle θ are provided (i.e., $\zeta_i^p = (\rho_i, \theta_i)^T$), the model, $\hat{\zeta}_i^p = (\hat{\rho}_i, \hat{\theta}_i)^T$, is given by³:

$$\hat{\rho}_i = \sqrt{(\Delta\hat{\alpha}_{*i}^p)^2 + (\Delta\hat{\delta}_i^p)^2}, \quad (23)$$

$$\hat{\theta}_i = \text{atan2}(\Delta\hat{\alpha}_{*i}^p, \Delta\hat{\delta}_i^p). \quad (24)$$

5 Detection limit of Gaia

By measuring the astrometry for one billion stars to a precision as high as $20 \mu\text{as}$, Gaia brings a new era of exoplanet detection. The expected sensitivity of Gaia and exoplanets with known absolute masses are shown in Fig. 5. To estimate the sensitivity region of Gaia in the m-a diagram, the astrometric signature of a reflex motion is given by:

$$\alpha_{\text{astro}} = \left(\frac{m_p}{m_s}\right) \left(\frac{a_p}{1 \text{ au}}\right) \left(\frac{d}{1 \text{ pc}}\right)^{-1} \text{ arcsec}. \quad (25)$$

When the observation baseline T is less than half of the orbital period P , the signature is

$$\alpha_{\text{astro}} = \left(\frac{m_p}{m_s}\right) \left(\frac{a_p}{1 \text{ au}}\right) \left(\frac{d}{1 \text{ pc}}\right)^{-1} \left\{ 1 - \sin \left[\pi \left(\frac{1}{2} - \frac{T}{P} \right) \right] \right\} \text{ arcsec}. \quad (26)$$

The signal to noise ratio (SNR) is defined as

$$\text{SNR} \equiv \alpha_{\text{astro}} / \sigma_{\text{fov}}, \quad (27)$$

where σ_{fov} is the along-scan accuracy per field of view crossing. Following Perryman et al. (2014), σ_{fov} can be approximately derived from the precision of parallax σ_{ϖ} following

$$\sigma_{\text{fov}} \approx 3.2\sigma_{\varpi}. \quad (28)$$

Assuming $\text{SNR} > 5$ as the detection threshold and adopting precisions of 30, 10, and $7 \mu\text{as}$ for the third, fourth, and fifth Gaia data releases (DR3, DR4, and DR5) respectively, as reported by Gaia Collaboration et al. (2023b) for bright stars, the detection limits of different Gaia data releases for a Sun-like star at a distance of 10 pc are shown in Fig. 5. While Gaia DR3 can barely detect Jupiter analogs, Gaia DR4 and DR5 are sensitive to Jupiter and even Saturn analogs. According to Perryman et al. (2014), Gaia would eventually detect more than 10,000 exoplanets.

Moreover, the astrometry detection method is sensitive to nearby exoplanets on wide orbits ($a > 1 \text{ au}$ or $P > 1 \text{ yr}$). This regime overlaps with the sensitivity ranges of both radial velocity and direct imaging methods. As a result, these techniques are commonly integrated to identify exoplanets characterized by exceptionally broad orbits and orbital periods spanning decades.

6 Conclusions

In recent years, advancements in technology, such as drift-scan astrometry and interferometry, have allowed for the measurement of stellar positions with sub-mas precision. With a precision in star position measurement as fine as $20 \mu\text{as}$, Gaia is anticipated to identify over 10,000 exoplanets, predominantly cold giant planets, by the conclusion of its mission. This level of precision is approaching the μas precision required for detecting nearby Earth-like planets around Sun-like stars. Looking ahead, the synergy between absolute and relative astrometry, such as combined analyses of

³The $\text{atan2}(y, x)$ function calculates the angle, in radians, between the positive x-axis and the ray extending from the origin to a point in the Cartesian plane.

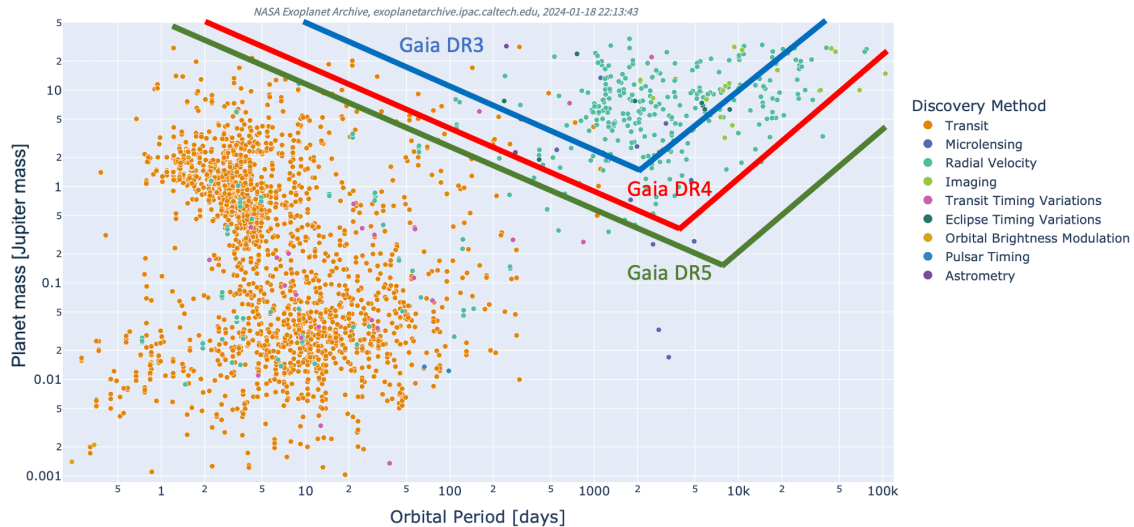


Fig. 5 Distribution of the currently detected exoplanets over orbital period and absolute planet mass. The mass for planets with orbital periods longer than 1000 days, discovered by radial velocity, is typically determined through combined analyses of radial velocity data and astrometric data from Gaia and Hipparcos. The detection limits of various Gaia data releases for a Sun-like star at a distance of 10 pc are presented by lines with different colors. It's important to note that the sample comprises known exoplanets obtained from NASA Exoplanet Archive, and none of the exoplanets displayed in this figure were newly discovered by Gaia.

FGS/HST and Gaia data, holds the potential to significantly enhance the observational baseline of astrometry. This improvement is crucial for detecting exoplanets, particularly those on extremely wide orbits.

Acknowledgments

This work is supported by Shanghai Jiao Tong University 2030 Initiative. I express my gratitude to my students, Guangyao Xiao and Yifan Xuan, for providing valuable comments on the manuscript.

References

- Benedict GF, McArthur B, Chappell DW, Nelan E, Jefferys WH, van Altena W, Lee J, Cornell D, Shelus PJ, Hemenway PD, Franz OG, Wasserman LH, Duncombe RL, Story D, Whipple AL and Fredrick LW (1999), Aug. Interferometric Astrometry of Proxima Centauri and Barnard's Star Using HUBBLE SPACE TELESCOPE Fine Guidance Sensor 3: Detection Limits for Substellar Companions. *AJ* 118 (2): 1086–1100. doi:10.1086/300975. astro-ph/9905318.
- Benedict GF, McArthur BE, Fredrick LW, Harrison TE, Slesnick CL, Rhee J, Patterson RJ, Skrutskie MF, Franz OG, Wasserman LH, Jefferys WH, Nelan E, van Altena W, Shelus PJ, Hemenway PD, Duncombe RL, Story D, Whipple AL and Bradley AJ (2002), Sep. Astrometry with the Hubble Space Telescope: A Parallax of the Fundamental Distance Calibrator δ Cephei. *AJ* 124 (3): 1695–1705. doi:10.1086/342014. astro-ph/0206214.
- Benedict GF, McArthur BE, Nelan EP and Harrison TE (2017), Jan. Astrometry with Hubble Space Telescope Fine Guidance Sensors—A Review. *PASP* 129 (971): 012001. doi:10.1088/1538-3873/129/971/012001. 1610.05176.
- Brandt TD, Dupuy TJ and Bowler BP (2019), Oct. Precise Dynamical Masses of Directly Imaged Companions from Relative Astrometry, Radial Velocities, and Hipparcos-Gaia DR2 Accelerations. *AJ* 158 (4), 140. doi:10.3847/1538-3881/ab04a8. 1811.07285.
- Charlot P, Jacobs CS, Gordon D, Lambert S, de Witt A, Böhm J, Fey AL, Heinkelmann R, Skurikhina E, Titov O, Arias EF, Bolotin S, Bourda G, Ma C, Malkin Z, Nothnagel A, Mayer D, MacMillan DS, Nilsson T and Gaume R (2020), Dec. The third realization of the International Celestial Reference Frame by very long baseline interferometry. *A&A* 644, A159. doi:10.1051/0004-6361/202038368. 2010.13625.
- Feng F, Lisogorskiy M, Jones HRA, Kopeikin SM, Butler RP, Anglada-Escudé G and Boss AP (2019), Oct. PEXO: A Global Modeling Framework for Nanosecond Timing, Microarcsecond Astrometry, and $\mu\text{m s}^{-1}$ Radial Velocities. *ApJS* 244 (2), 39. doi:10.3847/1538-4365/ab40b6. 1910.01750.
- Feng F, Butler RP, Vogt SS, Clement MS, Tinney CG, Cui K, Aizawa M, Jones HRA, Bailey J, Burt J, Carter BD, Crane JD, Dotti FF, Holden B, Ma B, Ogihara M, Oppenheimer R, O'Toole SJ, Shectman SA, Wittenmyer RA, Wang SX, Wright DJ and Xuan Y (2022), Sep. 3D Selection of 167 Substellar Companions to Nearby Stars. *ApJS* 262 (1), 21. doi:10.3847/1538-4365/ac7e57. 2208.12720.
- Gaia Collaboration, Prusti T, de Bruijne JHJ, Brown AGA and et al. (2016), Nov. The Gaia mission. *A&A* 595, A1. doi:10.1051/0004-6361/201629272. 1609.04153.
- Gaia Collaboration, Klioner SA, Lindegren L, Mignard F and et al. (2022), Nov. Gaia Early Data Release 3. The celestial reference frame (Gaia-CRF3). *A&A* 667, A148. doi:10.1051/0004-6361/202243483. 2204.12574.
- Gaia Collaboration, Arenou F, Babusiaux C, Barstow MA, Faigler S, Jorissen A and et al. (2023a), Jun. Gaia Data Release 3. Stellar multiplicity, a teaser for the hidden treasure. *A&A* 674, A34. doi:10.1051/0004-6361/202243782. 2206.05595.
- Gaia Collaboration, Vallenari A, Brown AGA, Prusti T and et al. (2023b), Jun. Gaia Data Release 3. Summary of the content and survey properties. *A&A* 674, A1. doi:10.1051/0004-6361/202243940. 2208.00211.

- GRAVITY Collaboration, Nowak M, Lacour S, Mollière P and et al. (2020), Jan. Peering into the formation history of β Pictoris b with VLTI/GRAVITY long-baseline interferometry. *A&A* 633, A110. doi:10.1051/0004-6361/201936898. 1912.04651.
- Gysembergh V, J. Williams P and Zingg E (2022). New evidence for hipparchus' star catalogue revealed by multispectral imaging. *Journal for the History of Astronomy* 53 (4): 383–393.
- Ho PY (2000). Li, Qi and Shu: An introduction to science and civilization in China, Courier Corporation.
- Jao WC, Henry TJ, Subasavage JP, Bean JL, Costa E, Ianna PA and Méndez RA (2003), Jan. The Solar Neighborhood. VII. Discovery and Characterization of Nearby Multiples in the CTIO Parallax Investigation. *AJ* 125 (1): 332–342. doi:10.1086/345515.
- Jefferys WH, Fitzpatrick MJ and McArthur BE (1988), Jan. GaussFit—A system for least squares and robust estimation. *Celestial Mechanics* 41 (1-4): 39–49. doi:10.1007/BF01238750.
- Kervella P, Arenou F, Mignard F and Thévenin F (2019), Mar. Stellar and substellar companions of nearby stars from Gaia DR2. Binarity from proper motion anomaly. *A&A* 623, A72. doi:10.1051/0004-6361/201834371. 1811.08902.
- Klioner SA and Kopeikin SM (1992), Aug. Microarcsecond Astrometry in Space: Relativistic Effects and Reduction of Observations. *AJ* 104: 897. doi:10.1086/116284.
- Miles BE, Biller BA, Patapis P and et al. (2023), Mar. The JWST Early-release Science Program for Direct Observations of Exoplanetary Systems II: A 1 to 20 μm Spectrum of the Planetary-mass Companion VHS 1256-1257 b. *ApJL* 946 (1), L6. doi:10.3847/2041-8213/acb04a. 2209.00620.
- Perryman MAC, Lindegren L, Kovalevsky J, Hoeg E, Bastian U, Bernacca PL, Crézé M, Donati F, Grenon M, Grewing M, van Leeuwen F, van der Marel H, Mignard F, Murray CA, Le Poole RS, Schrijver H, Turon C, Arenou F, Froeschlé M and Petersen CS (1997), Jul. The HIPPARCOS Catalogue. *A&A* 323: L49–L52.
- Perryman M, Hartman J, Bakos GÁ and Lindegren L (2014), Dec. Astrometric Exoplanet Detection with Gaia. *ApJ* 797, 14. doi:10.1088/0004-637X/797/1/14. 1411.1173.
- Snellen IAG and Brown AGA (2018), Aug. The mass of the young planet Beta Pictoris b through the astrometric motion of its host star. *Nature Astronomy* 2: 883–886. doi:10.1038/s41550-018-0561-6. 1808.06257.
- Thiele TN (1883), Jan. Neue Methode zur Berechnung von Doppelsternbahnen. *Astronomische Nachrichten* 104: 245.